Electronic Supporting Information

Photothermal Synergistic Nitric Oxide Controlled Release Injectable Self-Healing Adhesive Hydrogel for Biofilm Eradication and Wound Healing

Weiling Peng,[a] Lixia Li,[a] Yu Zhang,[a] Haibin Su,[a] Xiaohe Jiang,[a] Haimeng Liu,[a] Xiaohua Huang,[a*] Li Zhou,[a] Xing-Can Shen,[b] and Chanjuan Liu[a*]

[a.] Guangxi Colleges and Universities Key Laboratory of Natural and Biomedical Polymer Materials, Guangxi Key Laboratory of Optical and Electronic Materials and Devices, and College of Materials Science and Engineering, Guilin University of Technology, Guilin 541004, P. R. China.

[b.] State Key Laboratory for Chemistry and Molecular Engineering of Medicinal Resources, School of Chemistry and Pharmaceutical Science, Guangxi Normal University, Guilin, 541001, China.

Keywords: Bacterial affinity; Mild-temperature photothermal therapy; Nitric oxide controlled release; Biofilm eradication; Wound healing promotion

Part of the experimental section:

Materials: Dopamine hydrochloride, 1,3,5-trimethylbenzene (TMB, 97.0%), tris(hydroxymethyl)-aminomethane (Tris, 99.9%), N, N'-di-sec-butyl-1,4-phenylenediamine (BPA, 96.0%), 1-ethyl-(3-dimethylaminopropyl) carbodiimide hydrochloride (EDC), N-hydroxysuccinimide (NHS), 4-carboxyphenylboronic acid (PBA), tannic acid (TA) and morpholine ethanesulfonic acid (MES) were purchased from Aladdin Industrial Co. (Shanghai, China). Pluronic F127, chitosan (CS) with a degree of deacetylation of ≥ 95.0% and a molecular weight of 32.7 KDa determined from viscosity method, and 2,2-biphenyl-1-picrylhydrazyl (DPPH) were bought from Shanghai Macklin Biochemical Co., Ltd. Glycidyltrimethylammonium chloride (GTMAC，≥ 95.0%) was purchased from Shanghai Adamas Reagent Co., Ltd. The NO detection kit (Griess reagent) was purchased from Shanghai Beyotime Biotechnology. Staphylococcus aureus (S. aureus, CMCC26003) was provided by Shanghai Luwei Microbial Science and Technology Co. Tryptone soy broth (TSB) and Crystal violet staining solution (2.5%) were obtained from Beijing Solarbio Science & Technology Co., Ltd.

Characterization: The morphology and size of the mesoporous polydopamine nanoparticles (MPDA NPs) were observed by transmission electron microscopy (TEM, JEOL 2100, Japan). Absorption spectra were measured by an ultraviolet-visible-near infrared (UV-vis-NIR) spectrometer (UV-2600, Shimadzu, Japan), and IR spectra were obtained by a Fourier transform infrared spectrometer (FTIR, Thermo Nexus 470, USA). The chemical structures of the samples were tested on

an Avance 500 MHz NMR spectrometer (Bruker, MA, USA). The size distribution of MPDA NPs was measured using Malvern Zetasizer (Nano ZS, Malvern, UK). The pore size distribution and specific surface area of MPDA nanoparticles were analyzed utilizing nitrogen adsorption isotherms by Brunauer-Emmett-Teller (BET, Micromeritics ASAP2010, USA). The morphology of the samples was observed by scanning electron microscopy (SEM, S4800, JEOL, Japan) operating at 5 kV. Rheological tests were carried out on a TA AR1500EX rotational rheometer using a 25 mm parallel plate with a fixed gap of 0.8 mm.

Synthesis of quaternized chitosan: Quaternized chitosan was derived from the modification of chitosan with GTMAC.[1] 1.0 g chitosan was suspended in 36 mL distilled water and added with 180 μL glacial acetic acid. After stirring for 30 min, GTMAC was added dropwise into the chitosan glacial acetic acid mixture. The molar ratio of GTMAC to amino groups on the chitosan backbone was 1:1. After the reaction mixtures were stirred at 55 °C for 18 h, the undissolved polymer was removed by centrifuging the mixture at 9000 rpm for 10 min at room temperature. The supernatant was precipitated by adding dropwise to a pre-cooled acetone / ethanol mixture (1:1, v / v). For purification, the product was dissolved in DI water and dialyzed exhaustively (MWCO 3500) against deionized water for one week. After lyophilization, the resultant QCS was obtained, and the chemical structure was confirmed by ^{1}H NMR solvation (dissolved in D_2O) and FTIR spectra.

Molecular weight determination: The molecular weight of QCS and QCS-TA

were measured by viscometry method.[2] Measuremnets were performed at 30 ± 0.5 °C with an Ubbelohde capillary viscometer with an inner diameter of 0.66 mm (Shanghai Qianfeng Rubber and Glass Company, China). The specific viscosity (η_{SP}) was measured at various concentrations (5.00, 3.33, 2.00, 1.43 and 1.25 mg mL^{-1}) and the intrinsic viscosity [η] obtained through extrapolation of the linear plot of η_{SP}/c versus c. The viscosity average molecular weight (Mv) was then calculated using the Mark-Houwink equation.[3]

Table S1. The experimental viscosity values and calculated molecular weight of QCS and QCS-TA.

Samples	Huggins' equations	R^2	[η]	Mv[a]
QCS	y =72247.72 x + 247.07	0.98726	247.07	33.2 KDa
QCS-TA	y =70187.86 x + 242.91	0.99397	242.91	32.6 KDa

[a] The molecular weight calculated by Mark-Houwink equation, $[\eta]=KM^{\alpha}$ (K and α are viscometry constants obtained based on literature.[3]

TA contents of the QCS-TA conjugates: The TA content in QCS-TA conjugates was determined by Folin-Cioalteu assay.[4] Briefly, 1.0 mL of QCS-TA solution (0.25 mg mL^{-1}) was thoroughly mixed with 2.5 mL of Folin-Ciocalteu reagent (10 times dilution) and incubated in the dark for 5 min at 30 ℃. Then, 4 mL of Na_2CO_3 solution (7.5%, w/v) was added and the mixture solution was incubated for 2 h in the dark. After that, the absorbance of the reaction mixture was measured at 760 nm. Meanwhile, the standard curve of TA was measured under the same reaction condition. Ultimately, the corresponding TA equivalent content in QCS-TA was calculated from the calibration curve of TA and the results were expressed as mg

of TA equivalent per g (mg TAE/g).

Evaluation of photothermal performance: The photothermal effect of MPDA under 808 nm laser irradiation (1.0 W cm^{-2}, 10 min) was evaluated using a NIR thermal camera (MAG30, Shanghai, China), where MPDA suspensions with different concentrations (0.1, 0.2, 0.4, 0.6 mg mL^{-1}) and power densities (0.5, 1.0, and 2.0 W cm^{-2}) were used. The temperature changes of MPDA were recorded, and the photothermal conversion efficiency (η) of MPDA was calculated via the following formula: [5]

$$\eta = \frac{hS\left(T_{max} - T_{surr}\right) - Q_0}{I\left(1 - 10^{-A_{808}}\right)} \quad (1)$$

$$\tau_s = \frac{mC_p}{hS} \quad (2)$$

$$Q_0 = hS\left(T_{max,water} - T_{surr}\right) \quad (3)$$

The value of τ_s (262.53) can be calculated from the linear regression curve in the cooling, which is the characteristic thermal time constant, m is the mass of MPDA NPs, and C_p is the heat capacity of water (4.2 J g^{-1} K^{-1}). Thus, the value of hS can be obtained. Then, Q_0 is calculated via equation (3), Where h is the heat transfer coefficient, S is the sample container surface area, $T_{max,\ water}$ represents the steady state maximum temperature of water and T_{surr} is the ambient temperature. Then the η can be calculated based on equation (1). T_{max} is the steady-state maximum temperature of the MPDA. I is the laser power, and A_{808} is the absorbance of MPDA at 808 nm.

The photothermal properties of QP/QT-MB hydrogel were also measured using

the same method of MPDA. For photothermal stability evaluation, the QP / QT-MB hydrogel was irradiated with an 808 nm laser (1.0 W cm^{-2}) for 10 min, and the laser was shut off to cool to room temperature. The heating and cooling process was repeated three times, and the temperature change of the QP/QT-MB hydrogel was recorded.

Mechanical properties of hydrogels: The compressive test was conducted using an electronic universal testing machine (MTS System, CMT2202) with a 10 N load cell. The hydrogels were prepared into cylinder shapes 6 mm in height and 10 mm in diameter) and compressed at a strain rate of 2 mm/min, and the strain varied from 0% - 80%, all these tests were employed more than 3 times.

Antioxidant efficiency of hydrogels: The antioxidant efficiency of hydrogels was evaluated by the DPPH free radical scavenging assay. Briefly, 100 μM DPPH and an amount of QP/QT and QP/QT-MB hydrogel (6.0 mg, 12.0 mg, 18.0 mg, 24.0 mg, and 60.0 mg) were dispersed in 3.0 mL of ethanol and incubated at room temperature for certain times. After centrifugation, the absorbance of the solution at 515 nm was measured by UV-vis spectrophotometer. The scavenging of DPPH was calculated by the following formula:[6]

$$DPPH\ scavenging\ \% = 1 - \frac{A_S - A_B}{A_C} \times 100$$

Where, A_S is the absorbance of the mixture containing the hydrogel and DPPH solution, A_B is the absorbance of the hydrogel after mixing with ethanol, and A_C is the absorbance of pure DPPH solution.

Swelling performance evaluation: The swelling ratio of hydrogel was measured

by gravimetric method, and the hydrogel samples were immersed in 20 mL of PBS (0.01 M, pH=7.4) at 37 ℃ for 24 h. After removing the solvent from the hydrogel surface with filter paper, the weight of the swollen hydrogel samples was weighed and recorded. The swelling ratio was calculated by the following equations:[7]

$$Swelling\ ratio = \frac{W_b}{W_a} \times 100\%$$

Where, W_b is the wet weight of the hydrogel after the swelling equilibrium and W_a is the weight of the hydrogel sample.

Water vapor transmission rate: Water vapor transmission rate (WVTR) of hydrogels was measured by standard method E96-00 at 37 ℃ and a relative humidity of 35%.[8] Firstly, the hydrogels (including QP/QT hydrogel, QP/QT-M hydrogel, QP/QT-MB hydrogel) were hermetically sealed on the opening holes of glass vials (diameter = 2.0 cm) containing 10 mL distilled water, and kept in a desiccator with a saturated solution of ammonium sulfate at 25 °C for 24 h. The water vapor can transfer through the exposed hydrogel area (3.14 cm^2) and the weight loss of vials was measured by a four-digit balance. Meanwhile, Tegaderm™ film and blank control (no covering) were also measured for comparison, all tests were carried out three times for each group. The WVTR was calculated according the following equation: $WVTR = (W_0\text{-}W_f) / tA$, Where A is area of the bottle mouth (m^2); t is the time (h), W_0 and W_f are the weights in g of the vials before and after being kept at 37 ℃ for 24 h, respectively.

In vitro biocompatibility evaluation: The cytotoxicity and hemolysis were used

for the biocompatibility assay of the obtained hydrogel in this work. The cytocompatibility of the hydrogel was evaluated by employing a leaching pattern test according reported in the literature.[9, 10] The sterilized QP/QT, QP/QT-M, and QP/QT-MB hydrogels were firstly immersed in the fresh DMEM medium for 24 h at 37 ^{o}C with shaking speed of 100 rpm, and then the mixture was centrifuged obtaining the supernatant as the extract solution. L929 cells were seeded at a density of 1.0×10^4 cells per well in 96-well plates. The cells were incubated for 24 h in DMEM media containing 10% FBS and 1% penicillin-streptomycin at 37 °C (5% CO_2). Next, the culture medium in each well was replaced by 200 μL of the fresh medium containing different concentrations of hydrogels leachate (the final hydrogels concentration in the medium is varied from 10 to 100, 500, 1000 and 2000 μg mL^{-1}). Then the cells were co-incubated with the hydrogel leching for another 12 h, after removing the culture medium and washing with PBS three times, the relative cell viability was determined by the standard MTT assay. The cells co-cultured with DMEM alone were used as the negative control group. The resultant absorbance values at 570 nm of the medium were acquired by a microplate reader. $Cell\ viability = (A_{hydrogel} / A_{control}) \times 100\%$, Where $A_{hydrogel}$ means the absorbance of hydrogel groups, and $A_{control}$ describes the absorbance of the control group. Furthermore, to visually detect cellular survival, the Live/dead stained assay was performed via co-staining the treated L929 cells with FDA (fluorescein diacetate) and PI (propidium iodide). Finally, it was observed using a fluorescence microscope (Olympus, CKX53).

For hemolysis assays,[1] erythrocyte was collected from the fresh mouse whole blood by centrifugation (1500 rpm, 5 min), the obtained erythrocytes were washed with 0.9% sodium chloride three times and then diluted to a concentration of 5% (v/v). After that, 500 mg of the sterilized QP/QT, QP/QT-M, and QP/QT-MB hydrogels were separately mixed with 500 μL of erythrocyte suspension in a 24-well culture plate and incubated at 37 °C for 2 h with a shaking speed of 100 rpm. The contents in the microplate wells were then centrifuged at 3000 rpm for 5 min, 100 μL of suspension was carefully transferred into another 96-well plate, and the absorbance of the supernatant at 540 nm was measured using a microplate reader (Multiskan FC, Thermo). As controls, the 0.9% sodium chloride (NS) and deionized water (DI) treatment groups were also performed as a negative control and a positive control, respectively. The experiment was repeated three times, and the hemolysis ratio was calculated as follows: *hemolysis ratio (%)* = $[(A_h - A_s)/(A_d - A_s)] \times 100\%$, where A_h is the OD value from the hydrogel groups, A_d is the OD value from the deionized water and A_s is the OD value from the 0.9% sodium chloride, respectively.

Hemostatic property of the hydrogel: All animal experimental procedures were performed according to the Guidelines for animal experimentation approved by the animal ethics committee of Guangxi Normal University, and male Kunming mice (7 weeks old, 20-25 g) obtained from Hunan SJA Laboratory Animal Co. Ltd were used throughout the study. The hemostatic properties of hydrogels were evaluated by using a mouse liver trauma model and a mouse tail amputation

model. In short, mice were anesthetized with 10% chloral hydrate and the hair on the abdomen was shaved. The liver was then exposed and the tissue fluid around the liver was wiped clean with filter paper. The weighed filter paper was placed under the liver, and a 1 cm wound was created in the liver and covered with hydrogel (200 μL). After 2 min, the weight of the filter paper that absorbed the blood was measured. The mouse tail amputation model was constructed by cutting the mouse tail at the middle position with a surgical scissor, and then 100 μL hydrogel was adhered to the wound site. The weight of the filter paper was measured after 2 minutes of absorption. In addition, commercially available medical gauze (Taizhou Xinkang Medical Materials Co., Ltd., China) and gelatin sponge (Xiang'en Medical Technology Development Co., Ltd.) as control groups, and no-treatment group as blank. All experiments were repeated 3 times.

Statistical analysis: Statistical Analysis: All quantitative data were presented as mean ± standard deviations (SDs). The statistical analysis between groups was evaluated by SPSS using one-way analysis of variance (ANOVA). The levels of significance were labeled with $*p < 0.05$, $**p < 0.01$, and $***p < 0.001$.

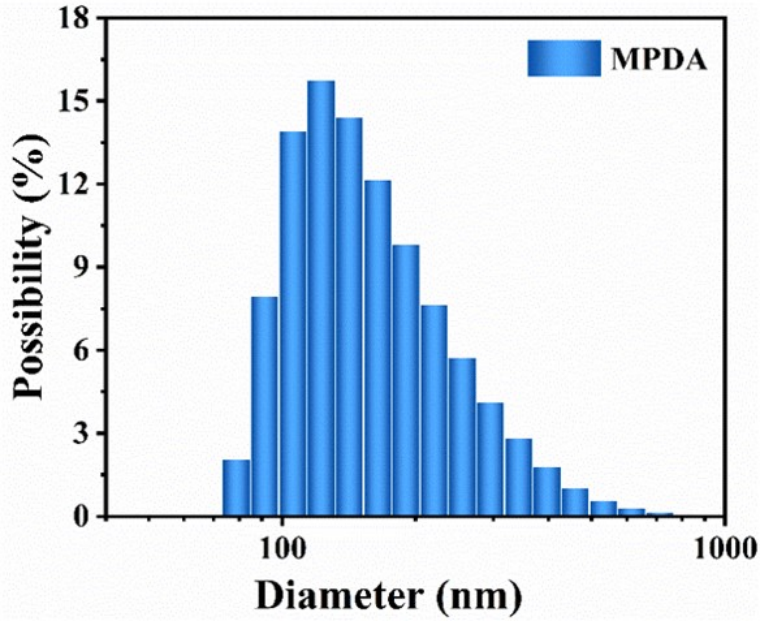

Figure S1 Hydrodynamic diameter distributions of MPDA suspended in deionized water.

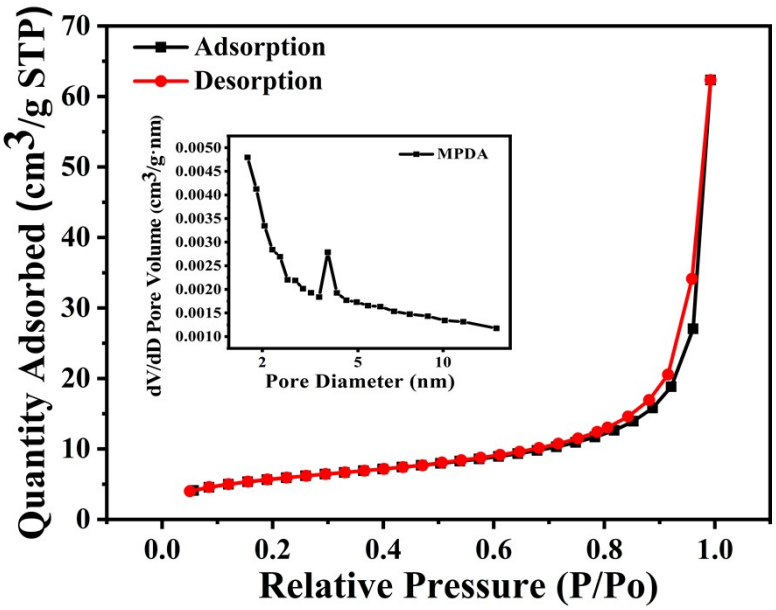

Figure S2 N_2 adsorption-desorption isotherm and pore size distribution curves of MPDA NPs.

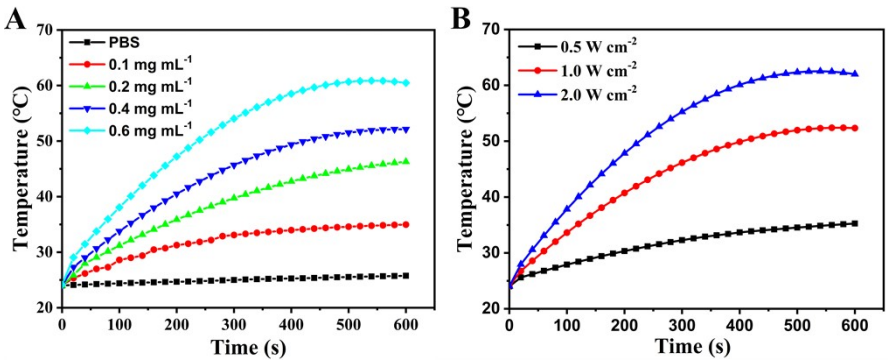

Figure S3 (A) Concentration-dependent temperature change curves of MPDA nanoparticle under NIR irradiation (808 nm, 1.0 W cm^{-2}). The temperature increased gradually with the increase of concentration and irradiation time. After 10 min of NIR laser irradiation, the temperature of different concentrations of MPDA solutions (0.1, 0.2, 0.4, and 0.6 mg mL^{-1}) increased rapidly from 24.0 °C to 35.0, 46.3, 52.1, and 60.5 °C, respectively. Whereas it only slightly increased to 25.8 °C for phosphate-buffered saline (PBS). (B) Temperature change of MPDA nanoparticles (0.4 mg mL^{-1}) with NIR irradiation (0.5, 1.0, and 2.0 W cm^{-2}). The change of temperature presented a power density-dependent photothermal performance.

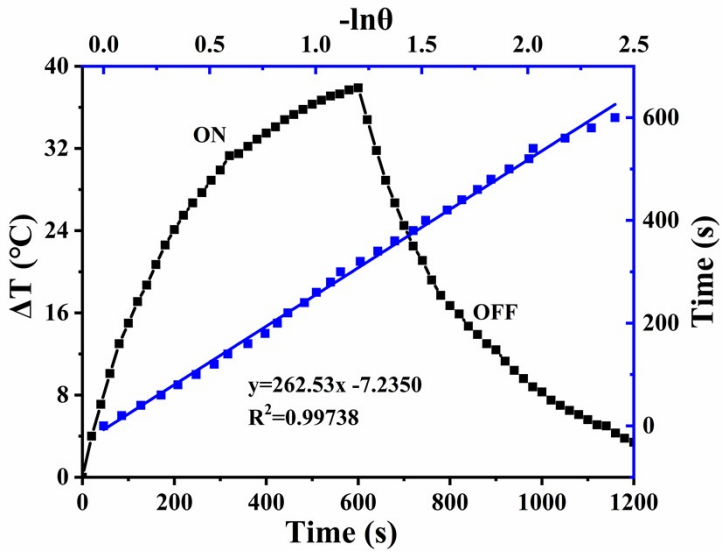

Figure S4 "On − off" temperature change of MPDA solution (0.6 mg mL^{-1}) under laser irradiation (black curve) and the cooling time plot versus -ln(θ) of MPDA (blue curve). Based on the heating-cooling curve and corresponding thermal time constant (τ_s), the η was ascertained to be 30.0%. The above results indicated the MPDA NPs effectively converted the NIR energy into heat energy.

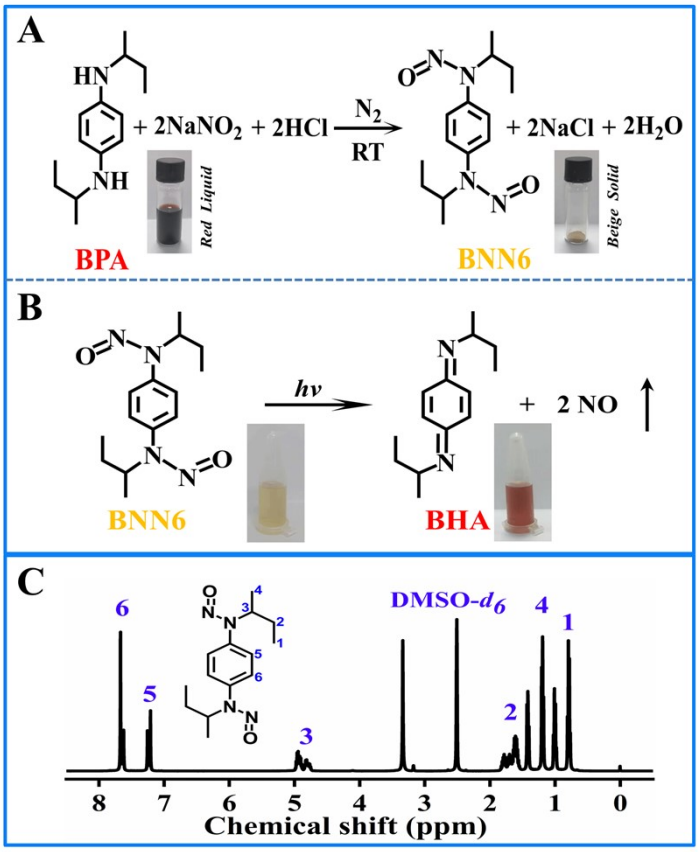

Figure S5 (A) Synthesis route of BNN6, it can be observed that the red liquid raw material becomes a pale yellow solid (inserted digital photo) after the reaction. (B) In the decomposition of BNN6 and generation of NO, it can be noticed that the color changes from colorless to red (dissolved in DMSO). (C) ^{1}H NMR spectrum of BNN6 (500 MHz, DMSO-d_6): δ 7.66 - 7.20 (m, 4H), 4.94 (d, J = 7.1 Hz, 2H), 1.60 (dd, J = 10.4, 7.2 Hz, 4H), 1.41 (t, J = 6.8 Hz, 2H), 1.18 (t, J = 6.7 Hz, 4H), 0.99 (q, J = 7.8 Hz, 2H), 0.78 (dd, J = 12.8, 7.2 Hz, 4H).

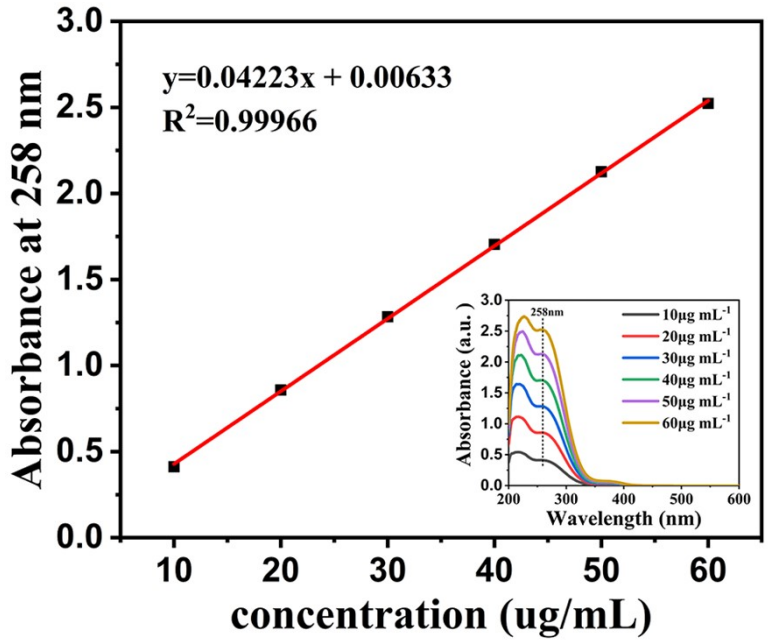

Figure S6 Standard curves of BNN6 (The inset shows the UV-vis absorption curve of BNN6 at different concentrations).

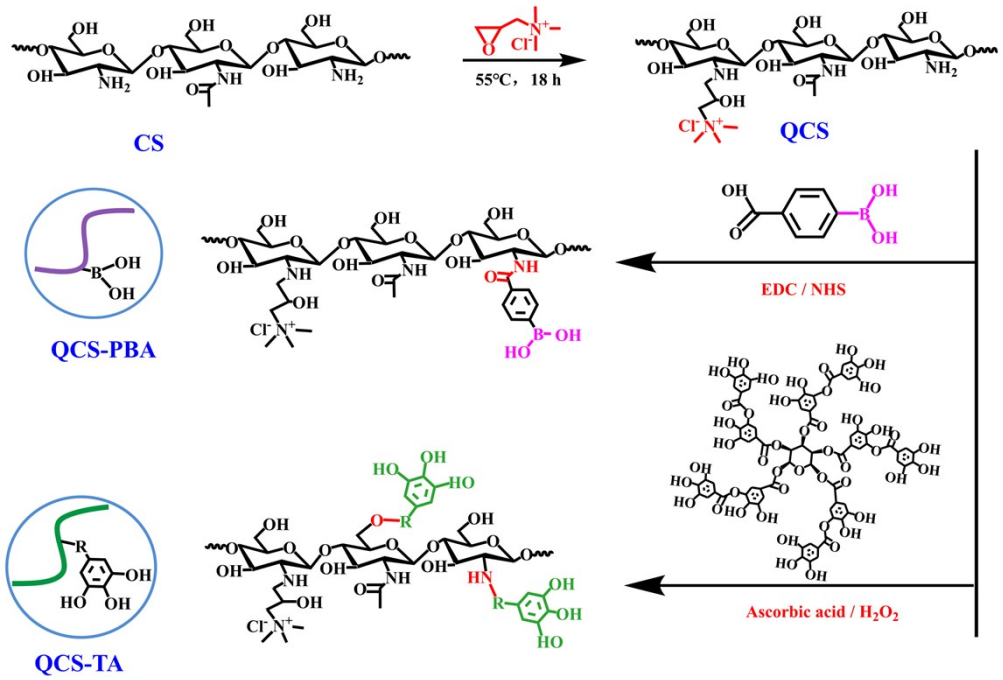

Figure S7 Synthesis of QCS, QCS-PBA and QCS-TA.

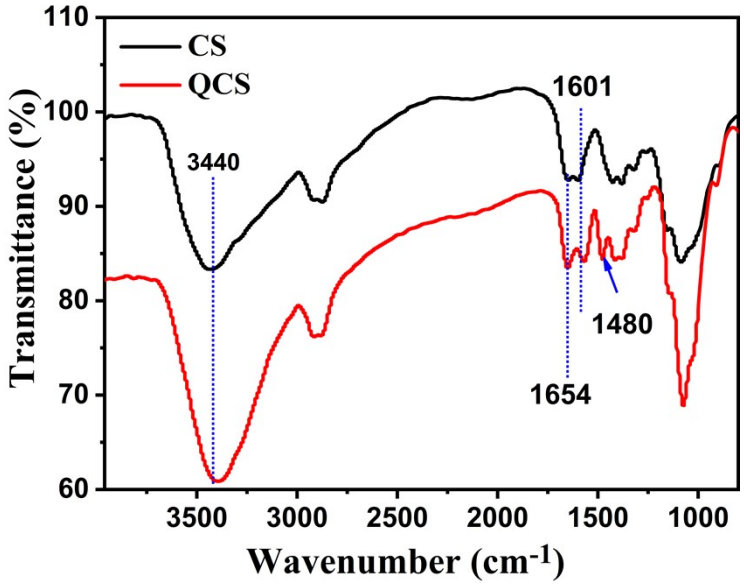

Figure S8 FTIR spectra of CS and QCS. The pristine CS showed a characteristic band at around 3440 cm^{-1} attributed to the combined peaks of the $–NH_2$ and –OH stretching vibration. The C=O stretching vibration of primary amide groups was located at 1654 cm^{-1}, as well as the N−H bending and C−N stretching vibrations of secondary amide groups were located at 1601 cm^{-1}. After the modification, this peak is weakened due to the consumption of some NH_2 groups through alkylation with trimethylammonium chloride, while a new sharp peak is observed at 1480 cm^{-1} corresponding to trimethylammonium groups.[11]

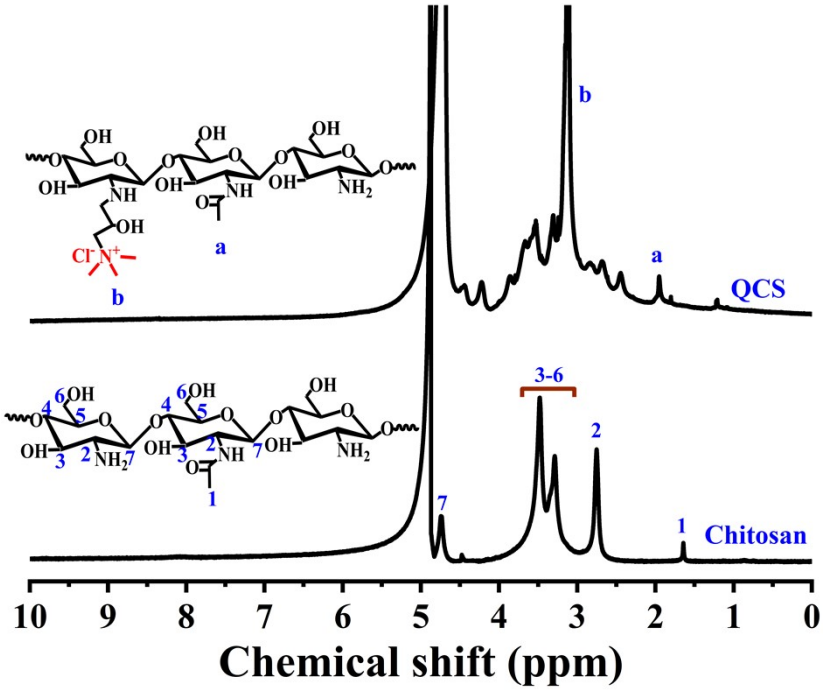

Figure S9 ^{1}H NMR spectra of CS and QCS. The characteristic peaks at 3.1 and 3.3 ppm were assigned to trimethylammonium and −NH−CH_2− groups, further proving the successful synthesis of QCS.

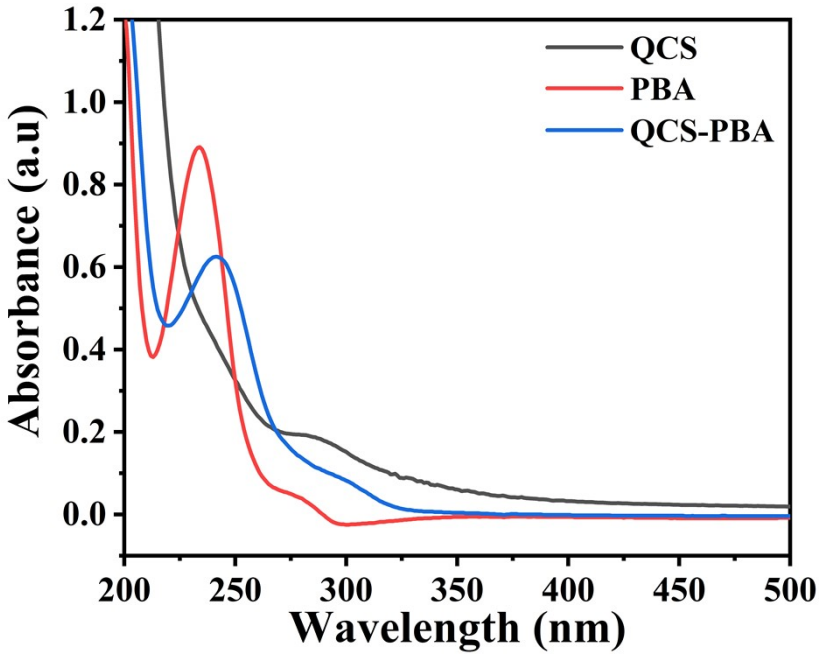

Figure S10 UV-vis spectra of QCS, PBA, and QCS-PBA.

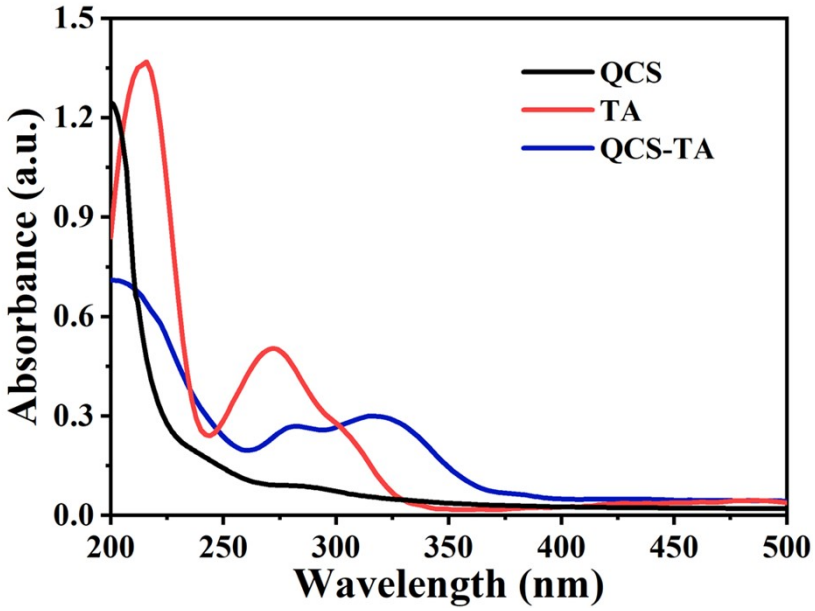

Figure S11 UV–vis spectra of QCS, TA and QCS-TA.

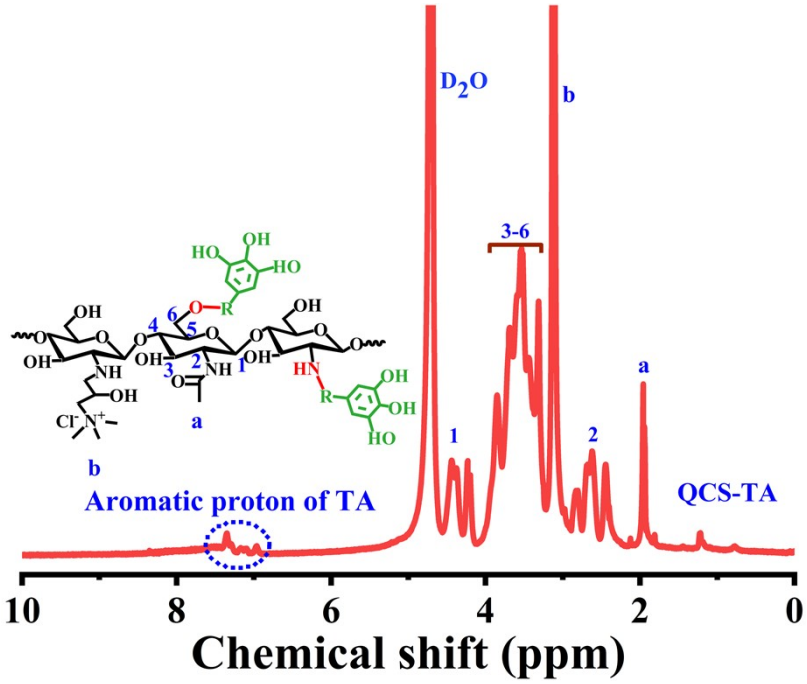

Figure S12 The ^{1}H NMR spectra of QCS-TA.

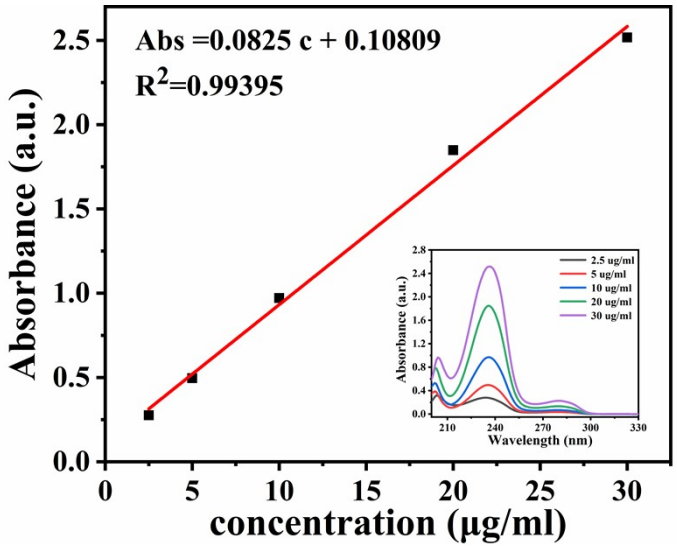

Figure S13 Standard curves of PBA, the inset presents the UV-vis spectra of PBA at different concentrations. The degree of PBA substitution was estimated to be 13.2% from the standard curve of PBA, which is in general consistent with the result obtained from ^{1}H NMR.

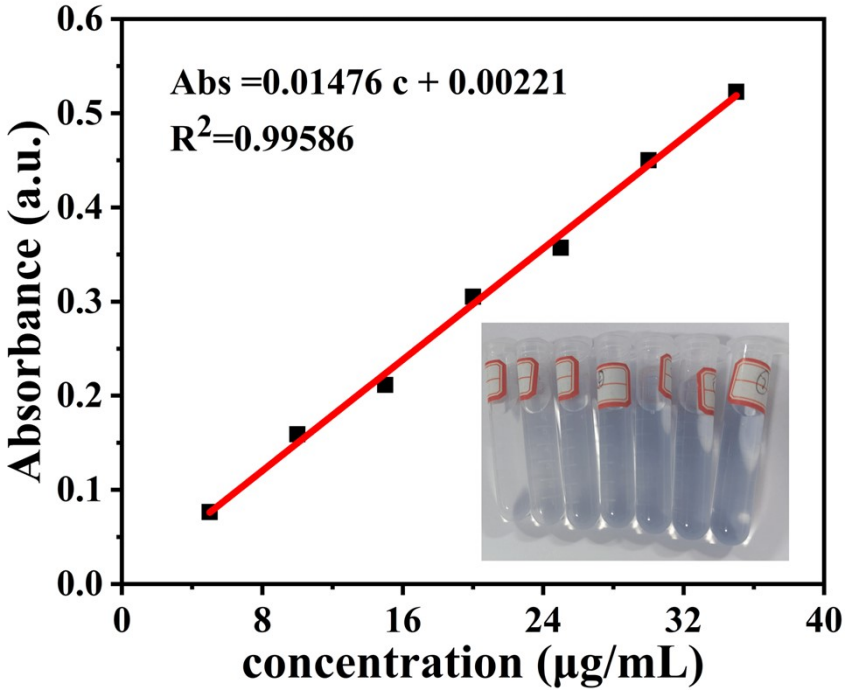

Figure S14 Standard calibration curve of tannic acids solutions.

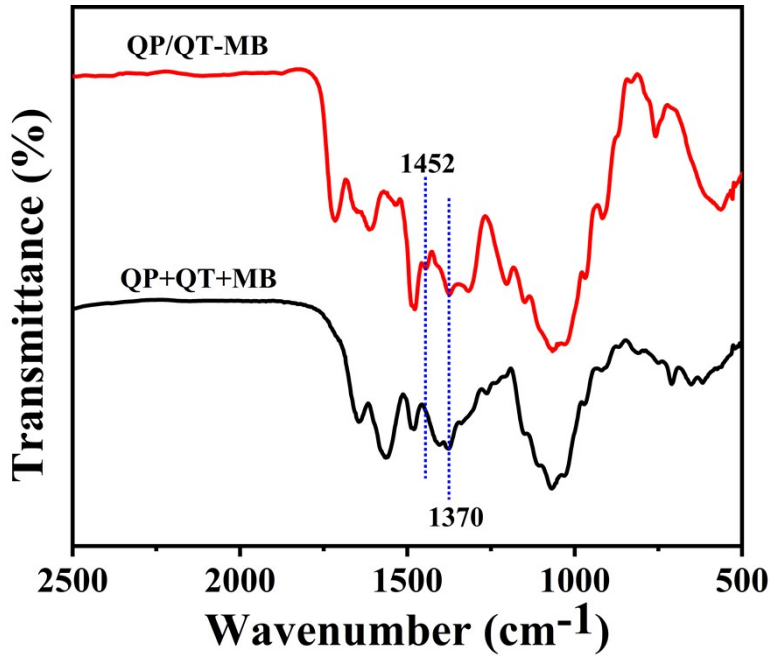

Figure S15 FTIR spectra of QP+QT+QB via simply mixed QP, QT, and MPDA@BNN6 and lyophilized QP/QT-MB hydrogel.

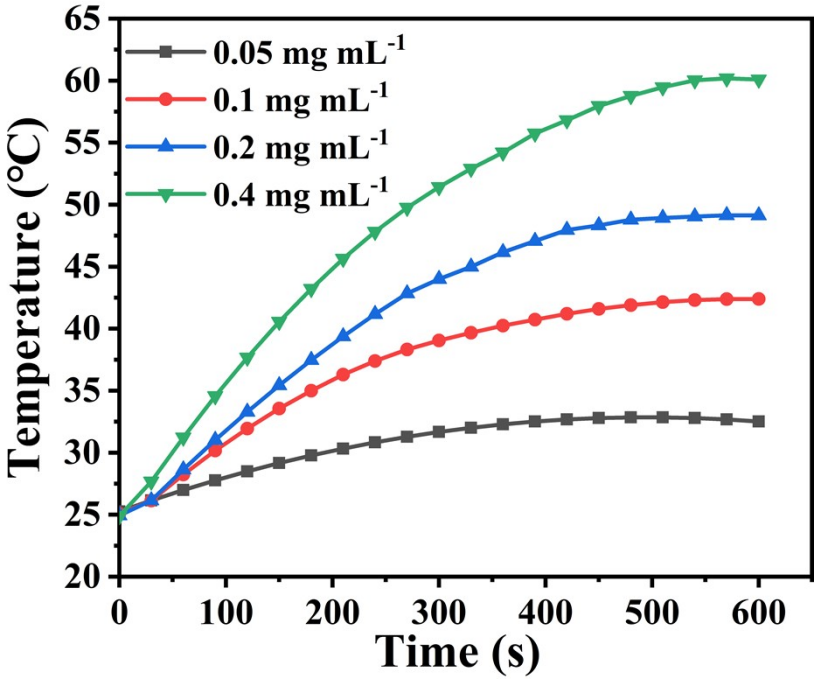

Figure S16 Photothermal heating curves of QP/QT-MB hydrogels with different MPDA concentrations under NIR irradiation (1.0 W cm^{-2}). The QP/QT-MB hydrogels embedded with different concentrations of MPDA@BNN6 (0.05, 0.1,

0.2, and 0.4 mg mL^{-1}) were exposed to 808 nm laser (1.0 W cm^{-2}, 10 min) and the temperature of the hydrogels was recorded with an IR camera. After 600 s NIR irradiation, the temperature rose to 32.5, 42.4, 49.1, and 60.0 °C, respectively.

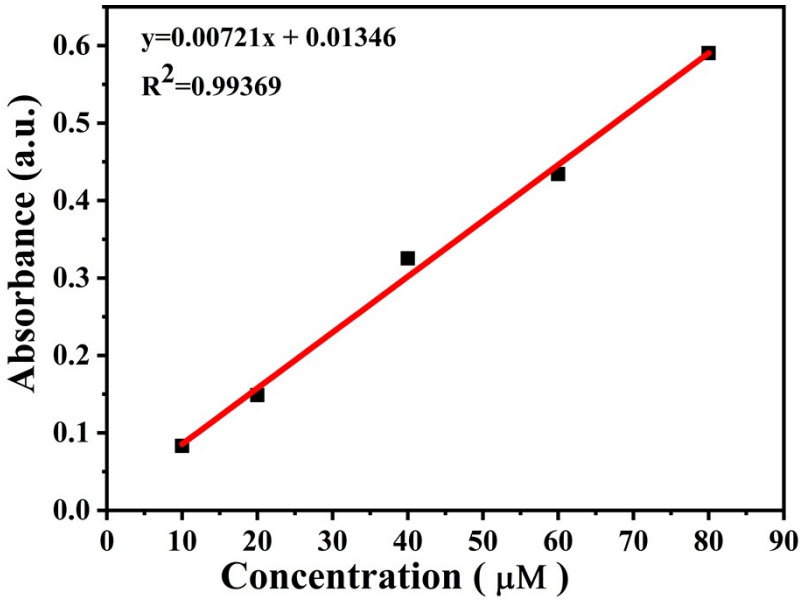

Figure S17 Standard curves for NO detection.

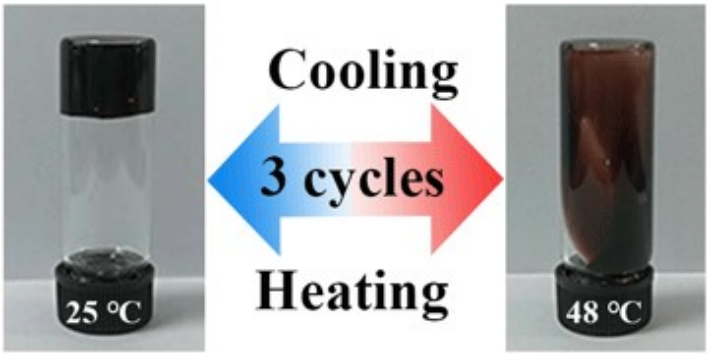

Figure S18 The thermo-sensitive and reversible gel-sol transition of the QP/QT-MB hydrogel. The hydrogel underwent a gel-sol transition when the temperature was over 48 ℃, and the converted sol gradually recovered to gel phase again during the cooling peroid even after 3 cycles.

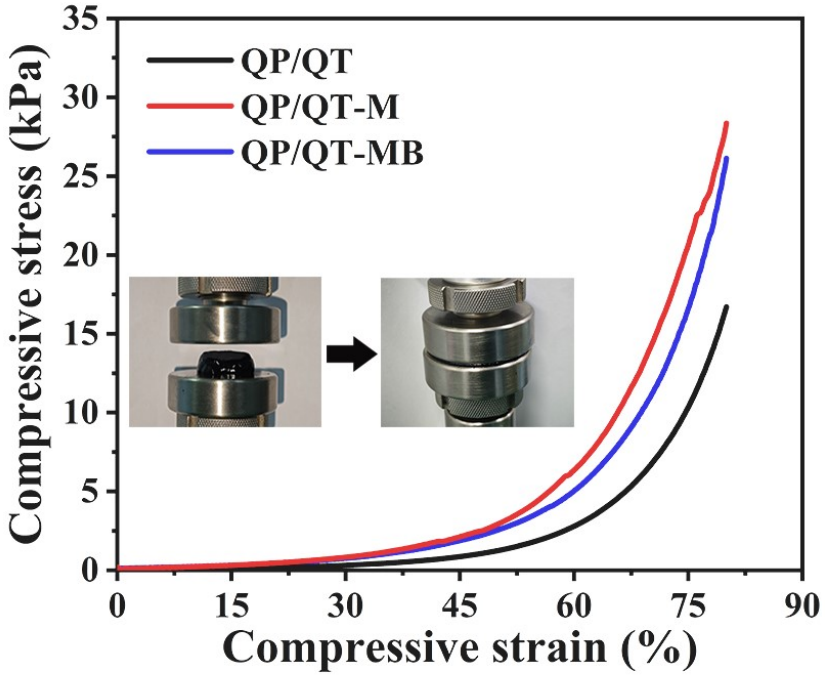

Figure S19 Compressive stress-strain curves of QP/QT, QP/QT-M and QP/QT-MB hydrogels.

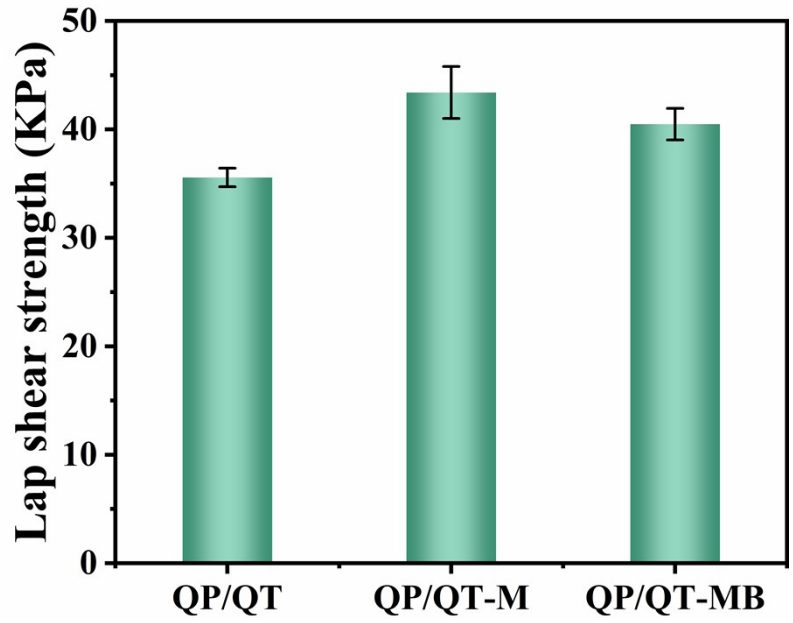

Figure S20 Adhesive strength of the QP/QT, QP/QT-M and QP/QT-MB hydrogels on pig skin.

Table S2 Adhesive performance of recently reported chitosan-based hydrogels.

Hydrogel	Adhesion components	Substrate	Adhesion strength	References
QP/QT-MB	TA	Porcine skin	40.0 kPa	this work
PBAM/CS/TFe	TA	Porcine skin	77.5 kPa	*ACS Appl. Mater. Interfaces*, 2022, **14**, 43010-43025
CS-LA	LA (α-Lipoic acid)	Porcine skin	41.0 kPa	*Chem. Eng. J.,* 2023, **470**, 143987.
QCS/TA	TA	Porcine skin	11.0 – 63.0 kPa	*ACS Appl. Mater. Interfaces,* 2022, **14**, 34455-34469.
HCS-PBA/CNTs-PDA	PDA	Porcine skin	27.6 kPa	*Appl. Mater. Today*, 2022, **26**,101362.
CS-GA	GA (gallic acid)	porcine skin	19.2 -84.7 kPa	*Chem. Eng. J.,* 2022, **427**, 130843.
PEGS-PBA-BA/CS-DA-LAG	DA (Dihydrocaffeic acid)	Porcine skin	17.5 kPa	*ACS Nano*, 2022, **16**, 3194-3207.
rGB/QCS/PDA–PAM	PDA	Porcine skin	16.3 kPa	*Adv. Sci.* 2023, **10**, 2206585.
Cs-Ph/Alg-Ty	TA	Porcine skin	1.4 - 16.1 kPa	*Carbohydr. Polym.,* 2022, **295**, 119844.
OSD/CMC/Fe/PA	DA	Porcine skin	8.0 kpa	*Bioactive Materials*., 2023, **30**, 129-141.
GT-AT/ACS/CD	Aldehyde	porcine skin	7.75-31.5 kPa	*Sci. China-Chem.,* 2022, **65**, 2238-2251.
PNIPAm-AA/QCS-CD/PPy	Adenine	Porcine skin	5.7 kPa	*Adv. Healthc. Mater.,* 2022, **11**, 2102749.
CS-HA/hmCS lactate	HA (Hydrocaffeic acid)	Porcine skin	3.8 - 8.2 kPa	*Biomacromolecules*, 2020, **21**, 1243-1253.

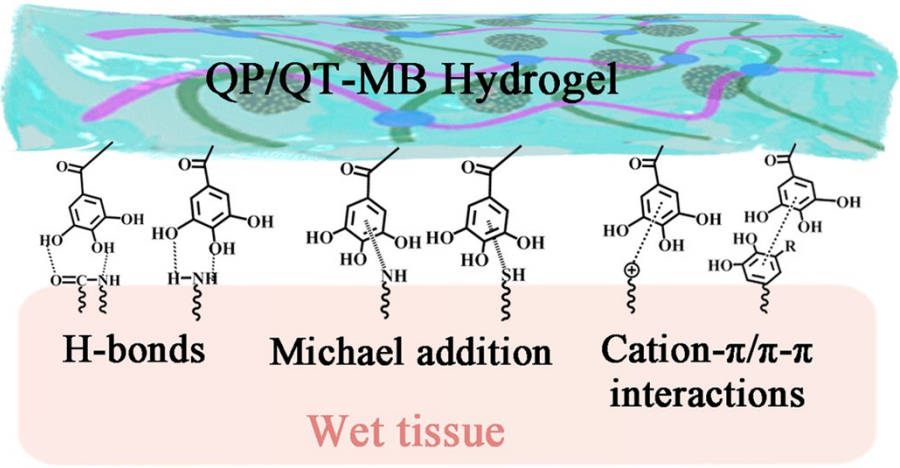

Figure S21 Adhesive mechanism of the hydrogel: the substantial catechol-like polyphenol moieties inside the hydrogel have the ability to form different types of covalent or / and noncovalent reactions with skin tissues, including hydrogen bonds, Michael addition, π–π / cation–π interactions.

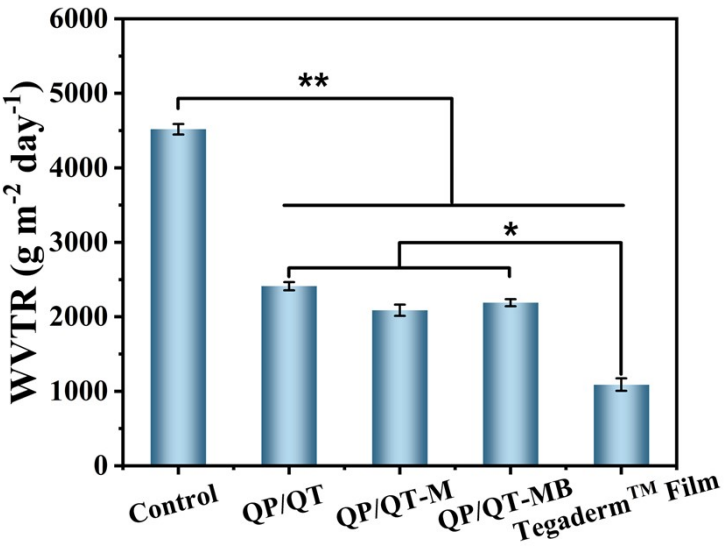

Figure S22 The water vapor transmission rate of QP/QT hydrogel, QP/QT-M hydrogel, and QP/QT-MB hydrogel, Tegaderm™ film and blank control (no covering). Data indicate mean ± SD (n=5). Error bar indicates standard deviation. *P < 0.05, **p < 0.01.

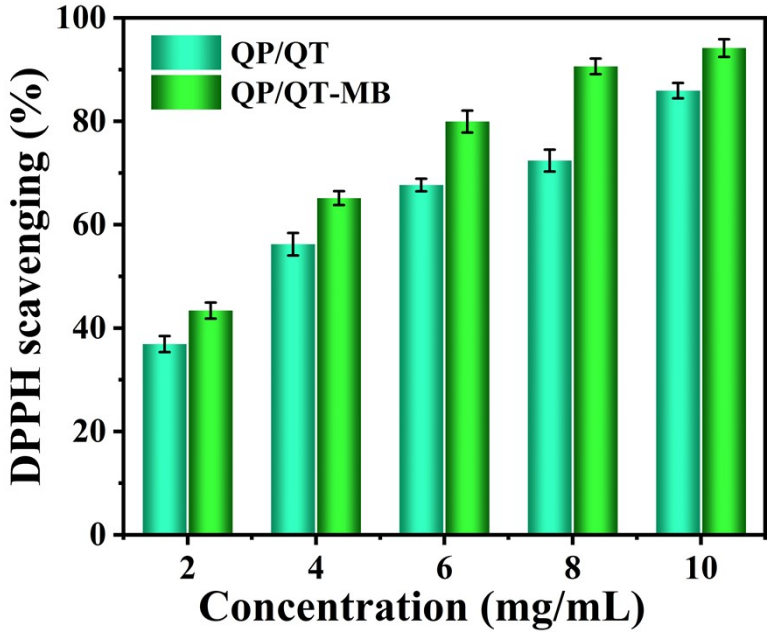

Figure S23 DPPH scavenging efficiency of QP/QT and QP/QT-MB hydrogels at different concentrations.

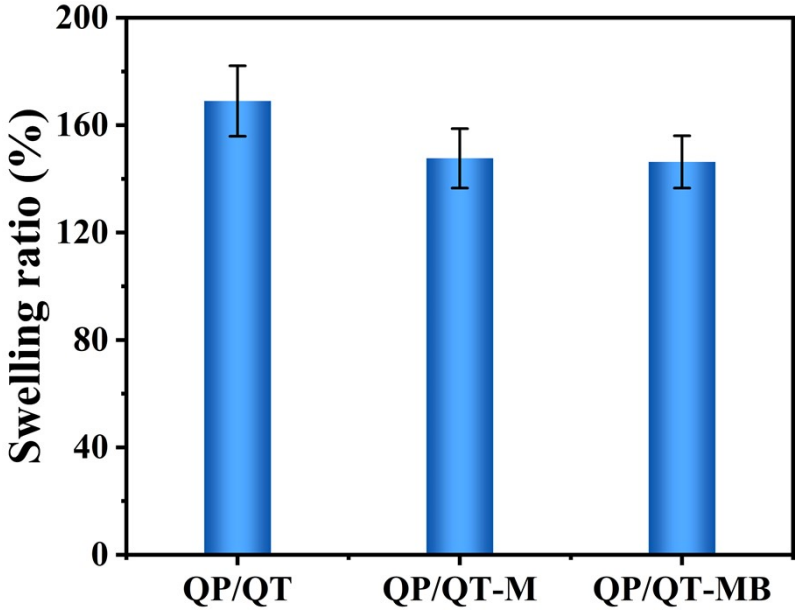

Figure S24 Swelling ratios of the QP/QT, QP/QT-M, and QP/QT-MB hydrogels.

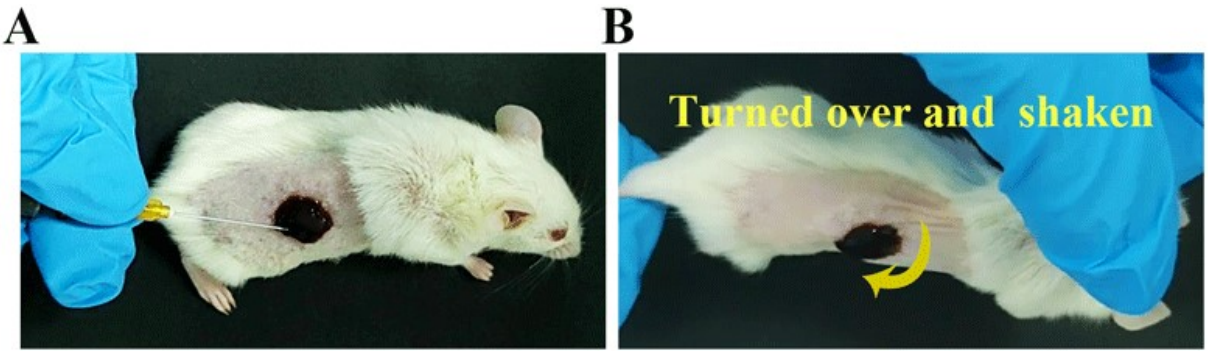

Figure S25 Photograph of the QP/QT-MB hydrogel injected into the infected wound (A), and the injected hydrogel fixed on the wound tissue that does not detach when the mouse was turned over and shaken (B).

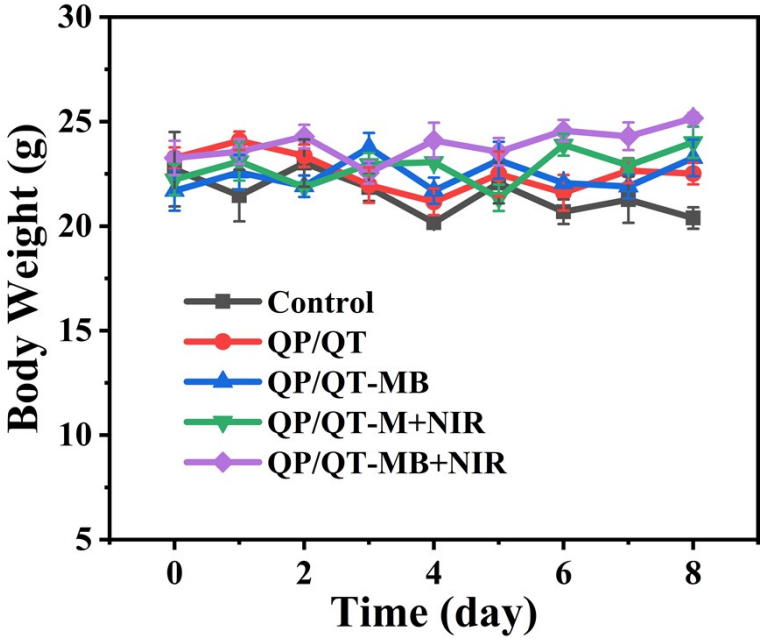

Figure S26 The weight change curve of mice in different treatment groups throughout the entire treatment process (n = 3).

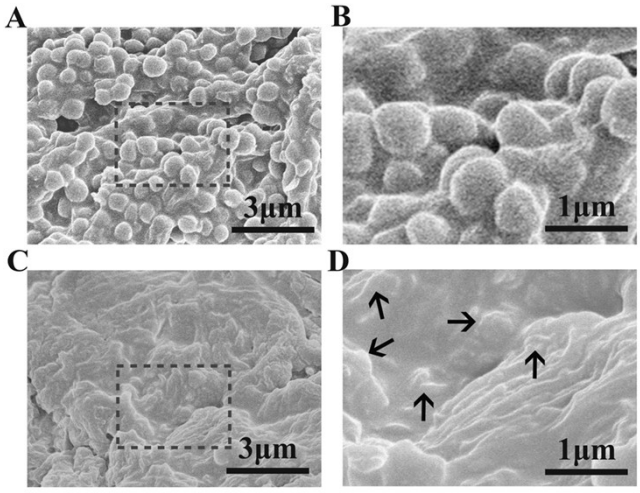

Figure S27 (A, B) SEM images of wound tissues before treatment with QP/QT-MB hydrogel dressing (scale bar: 3 μm; 1 μm); (C, D) SEM images of wound tissues after treatment with QP/QT-MB hydrogel dressing and irradiation with NIR laser (scale bar: 3 μm; 1 μm).

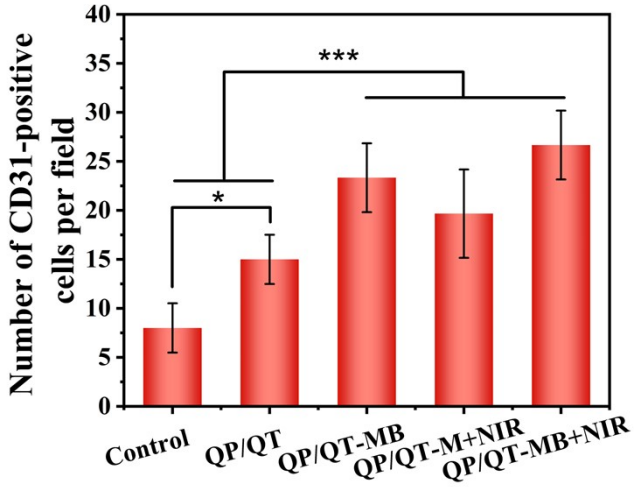

Figure S28 Quantitative statistical results of CD31-positive cells numbers in the wound tissues for each group after 8 days of treatment, n = 3, *p < 0.005, and ***p < 0.01. The vessel number in wound treated with QP/QT-MB+NIR was the largest with approximately 27 per field, while the other groups showed only approximately 24 (QP/QT-MB), 20 (QP/QT+NIR), 15 (QP/QT), and 8 (PBS) per field, respectively.

References

1. Y. Q. Liang, Z. L. Li, Y. Huang, R. Yu and B. L. Guo, *ACS Nano*, 2021, **15**, 7078-7093.
2. C. H. Wang, W. S. Liu, J. F. Sun, G. G. Hou, Q. Chen, W. Cong and F. Zhao, *Int. J. Biol. Macromol*., 2016, **84**, 418-427.
3. G. A. F. Roberts and J. G. J. I. J. o. B. M. Domszy, *Int. J. Biol. Macromol*., 1982, **4**, 374-377.
4. Y. M. Zheng, B. Y. Chen, X. X. Huang, H. Teng, C. Ai and L. Chen, *Ultrason. Sonochem*., 2023, **95**, 106396.
5. G. H. Liu, L. Wang, Y. He, L. C. Wang, Z. W. Deng, J. J. Liu, D. Peng, T. Ding, L. Lu, Y. Ding, J. X. Zhang, P. Liu and K.Y. Cai, *Adv. Healthc. Mater*., 2021, **10**, 2101476.
6. Y. J. Zhong, F. Seidi, Y. L. Wang, L. Zheng, Y. C. Jin and H. N. Xiao, *Carbohydr. Polym*., 2022, **298**, 120103.
7. P. P. Deng, X. Liang, F. X. Chen, Y. Chen and J. P. Zhou, *Appl. Mater. Today*, 2022, **26**, 101362.
8. T. C. Reis, S. Castleberry, A. M. B. Rego, A. Aguiar-Ricardo and P. T. Hammond, *Biomater. Sci*., 2016, **4**, 319-330.
9. Y. Huang, L. Mu, X. Zhao, Y. Han and B. L. Guo, *ACS Nano*, 2022, **16**, 13022-13036.
10. J. E. Cun, Y. Pan, Z. Z. Zhang, Y. Lu, J. H. Li, Q. Q. Pan, W. X. Gao, K. Luo, B. He and Y. J. Pu, *Biomaterials*, 2022, **287**,121687.
11. H. Xue, Z. H. Zhang, Z. Lin, J. Su, A. C. Panayi, Y. Xiong, L. C. Hu, Y. Q. Hu, L. Chen, C. C. Yan, X. D. Xie, Y. S. Shi, W. Zhou, B. B. Mi and G. H. Liu, *Bioact. Mater*., 2022, **18**, 552-568.